

# Experimental Research on Flow Characteristics close to Hydrophobic Surface

D. Jasikova, M. Kotek, S. Fialova, V. Kopecky

**Abstract**— Combination of hydrodynamic and mechanical specification of the flow can reach the complex description of the liquid flow in the hydraulic system. The initial condition is the flexible wall and hydrophobic surface of the model. The simplification of the system leads to primary setup focused in one direction. It is the hydrophobic surface in our case. Here we present the study based on four various set of samples. We worked with hydrophobic surfaces, with contact angle (CA) above 90°, and with ultra – hydrophobic surfaces with CA above 120°. Increasing the contact angle leads from bubbles conglomeration to uniform air film. Using visualization methods and PIV we studied the air film layer on the hydrophobic surface and determined the velocity profiles in the water channel covered with hydrophobic surface. The existence of symmetrical air film close to hydrophobic surface has an effect on the character of the velocity profile and its boundary slip condition.

**Keywords**— hydrophobic surface, particle image velocimetry, boundary condition, slip effect, pipe flow.

## I. INTRODUCTION

RECENT development of biomechanics and preparation of prostheses parts of organs contribute to the need for surface modification of traditional materials. The major condition is physiology most similar to natural materials. These include compensation vascular beds, the airways, and design of external device for securing vital functions, i.e. external blood circulation, ventilation system. [1-4]

The synergy effect of joining branches of research: biomechanics, material engineering and fluid mechanics bring success due the combination of knowledge. Contribution of fluid mechanics can imagine the equivalent of flow in arteries as the pipe flow, hence the Poiseuille's flow, with appropriate viscoelasticity and wettability against Newtonian and non-Newtonian liquids. [5]

The fluid mechanics has been solving issue of liquid flows on a model of rigid tubes. [6-8]

We have to follow the liquid characteristics. The natural liquids are not homogenous, but heterogeneous - multiphase

The authors gratefully thank to the support of Grant Agency of the Czech Republic (GA ČR) 17-19444S Interaction of heterogeneous liquid with flexible wall, and LO1201 co-funding from the Ministry of Education, Youth and Sports as part of targeted support from the „National Programme for Sustainability I“.

D. Jasikova, is with the Department of Physical Measurement, The Institute for Nanomaterials, Advanced Technology and Innovation, Technical University of Liberec, Studentska 1402/2, 46117 Liberec 1, Czech Republic (e-mail: darina.jasikova@tul.cz)

S. Fialova, Jr., is with Faculty of mechanical engineering, Brno University of Technology, Technicka 2896/0, Kralovo Pole, 61669, Brno, Czech Republic, (e-mail: fialova@fme.vutbr.cz).

flow. [9-15]

An important role in the study of hemo-transport has its interaction with walls. In reality, and in attempting to artificial substitutes should be envisaged wettability / hydrophobicity, that significantly affects the character of heterogeneous structures and character of fluid flow velocity profiles. [15-21]

In the initial step we start from a simplified model, we return back to solid walls and flow of Newtonian fluids. The main areas of interest of this part of the research are the effect of hydrophobicity on the flow velocity profile. S. Fialova and F. Pochly described condition of resistive forces during flow along the hydrophobic surface. These studies confirm defined conditions for fixed wall - slip effect in their previous work [22-26]. The manifestation of this effect is also described in E. E. Meyer as the solid-liquid interface interaction observed as slip length close to hydrophobic surfaces. [27]

The combination of hydrodynamic and mechanical specification of the flow can reach the complex description of the liquid flow in the hydraulic system. The initial condition is the flexible wall and hydrophobic surface of the model. The simplification of the system leads to primary setup focused in one direction. It is the hydrophobic surface in our case. As it was mentioned in previous studies, the interaction of liquid and hydrophobic surface is followed by the slip effect. Here we present the study based on four various samples to prove experimentally this condition.

## II. EXPERIMENTAL SETUP

The experimental setup was based on manufactured group of various samples each in four specimens: with non-modified surface, surface with ceramic cover, and hydrophobic surfaces. The hydraulic circuit was pressure driven, so we followed the decryption for Poiseuille's flow in pipe system. Stainless steel samples had diameter of inner channel (80 x 8 x 8) mm and were edgeless joined to the hydraulic circuit of entrance length over 500 mm. The inner duct was further surface modified using plasma treatment to increase the contact angle. The system was enhanced with a linear precision voltage source KORADO KA3005P controllable from a PC and an adjustable voltage with an accuracy of hundredths. The liquid - water was draw from the reservoir. The entrance length of the inlet straight duct was 1m as well as the strait part on the outlet from the channel.

One set of samples were inner coated with ceramic layer. This layer is very mechanically and chemically resistant but during preparation it requires high-temperature stabilization.

The contact angle (CA) of this cover is 100°. The ceramic cover can be further modified using both chemical and mechanical treatments. There is assumption of mechanical resistance and long life due the unique uniform microstructure of this material.

There was used product Ultra Ever Dry developed by UltraTech international, Inc. to obtain ultra-hydrophobic surface modification. We used this modification on rough steel samples as well as those with ceramic inner surface. The plasma pre-treatment preceded to ultra-hydrophobic modification. Electrodes were connected via an impedance matching unit to a radio frequency generator (Dressler) which is operated at a frequency of 13.56 MHz. The applied power was 300 W. Argon (99.996 % Erproduct) was used as a working gas delivered at a flow rate of 50 ml/s into the plasma jet. The super hydrophobic product was subsequently applied according to the instructions using a commercial spray device.

#### A. Measurement Technique

Choice of visualization and measurement methods followed the condition of the pipe flow (although square cross section) and complex information of the velocity profile in time. We came out from the Particle Image Velocimetry (PIV) technique modified to small scale measurement using long distance microscopy. The design of the measurement track and the samples were adapted to his method.

We set the system on NewWave Gemini Nd:YAG pulsed laser for the illumination of investigated area, energy up to 120mJ per pulse length of 10 ns, wavelength 532 nm. The images are captured with Neo CMOS chip 5.5 MPixel size of 6.5 microns camera. Laser and camera system is controlled from a computer and synchronized with the external TimerBox.

Unlike standard PIV method, where the depth of field depends on the distance to the measurement object from the camera lens, f-number, in the micro PIV method depth of field is dependent on the parameters of the microscope lens, index of refraction of the liquid, and the wavelength of used light. Other parameters are related to the system of lenses: NA - iris, M - total magnification microscope, and e - the distance between the pixels on the CCD camera.

The arrangement of micro PIV has a constant depth of field 4 μm at 4x magnification. This factor is important for choosing the size of seeding particles. Here in this investigating we used coated Rhodamine B 2 μm fluorescent particles emitting light on 570 nm. We used set of microscopic calibration targets for the calibration of the system to determine the magnitude coefficient.

The long distance microscopy method was used for the measurement of the velocity profile over the whole channel in one step. This optical setup was based on INFINIPROBE™ TS-160 universal macro/micro imaging system that enables 4 x magnifications. This probe was working in the set of compressor for the wide field of view, and the working distance was 100 mm in the macro regime. The area of interest was illuminated with the laser light led with optical cable towards the sample.

The measurements run at 8 Hz frequency with 60 mW laser power at one flash. The light from the laser head was brought to investigated area with optical cable. For each measurement at least 290 records were always acquired and were further processed by the correlation function, validation and filtering before being evaluated statistics and estimated velocity profiles..

### III. RESULTS AND DISCUSSION

It is known that amount of inert gases dissolved in the liquid as well as present micro-bubbles in the water at  $p = 105$  Pa at room temperature  $T = 298.15$  K is  $\alpha = 0.005$ . Once the water is boiled or pressurized the amount  $\alpha$  rapidly decrease. There exists  $1.12 \times 10^9$  nucleuses per  $m^3$  in untreated tap water and the most probable size is about  $6 \mu\text{m}$ . was observed by Brennen, as he reported, the cavitation inception number as a function of the Reynolds number [28,29] The number of nucleuses for pressured and ultrasound degassed water can decrease to  $3 \times 10^8$ .

Our research is also focused on hemo-transport, we are taking in account the real situation of gases dissolved in blood as well. We consider that 97% of oxygen is bond to hemoglobin, and 3% of oxygen is physically dissolved in 1 liter of blood plasma. It is also 12% of physically dissolved of CO<sub>2</sub> and 11% is bonded to carbaminohemoglobin. There is a balance between these two groups: dissolved and bounded gas that can be interrupted. In arterial blood there is 0.29 ml of O<sub>2</sub> dissolved in 100 ml of blood plasma. Following this physiology set the volume of dissolved gas corresponds to very well degassed water.

The blood flow can be seen as multi – phase flow from the view of experimental fluid mechanics. This flow is accompanied by different flow patterns. Blood's components are plasma and erythrocytes, from the very simplified view. The whole system contains gas. Even liquid contains gas in different state of aggregation can be observed as multi-phase flow. It is necessary to investigate the boundary condition before we start to examine flow pattern interactions. The wall boundary condition, especially in the system with surface structure modifications, has been not very well described yet. Actually, one boundary condition for flow patterns in pipe flow is surface friction, gradient of densities, and interfacial surface tension.

These stratified flows are objects of practical interest. From the analytical and mathematical point of view, it is a problem consisting of macroscopic predictions and microscopic modelling. Basically, the air film characteristics come from its geometry, symmetry, and Reynolds number presenting fluid flow. [28, 29] Anyway, for the correct analysis there has to be taken satisfactory quantity of experimental dataset.

Dissolved air is formed into more or less uniform air film. The formation of the air film is dependent on the flow pattern. The film structure is dependent on the geometry of the channel, roughness of the surface and it can be symmetrical or unsymmetrical. We can call it bubbly, slug, chum or annular flow. The annular flow develops, when it met the condition of hydrophobic surface. There is developing an air film close to

the inner walls.

It is said, that the air film thickness is dependent mostly on the channel geometry, that is represented by the hydraulic parameter  $D$  and  $\alpha$  is amount of the dissolved air, so we can estimate the relation  $d=D(1-\sqrt{1-\alpha})/2$ , but according to previous formulation, that the air film is dependent on the flow pattern, this can be expressed using Re number.

Following this formulation the interaction of the liquid flow and the air film can be divided into two regions:  $Re < 500$ , and  $Re > 500$ . In the first are acting macroscopic eddies instead of the second one with microscopic eddies. Anyway, here the interaction moved from the liquid/surface to gas/liquid interface. This theoretical description of the existence of the air film on hydrophobic surfaces had to be firstly proved its existence and demonstrated with the visualization technique. The microscopic view proved the local existence of the air film and allows further description of the effect.

The existence of the air film formation was proved with microscopic view. The film is formed in the region  $Re < 500$  and can be seen as light stripe that reflects the light. Images taken by camera connected to inverted microscope were analyzed with the methods of image processing. Several brightness profiles were taken across the image. Image data and result of the image processing is seen on Fig. 1.

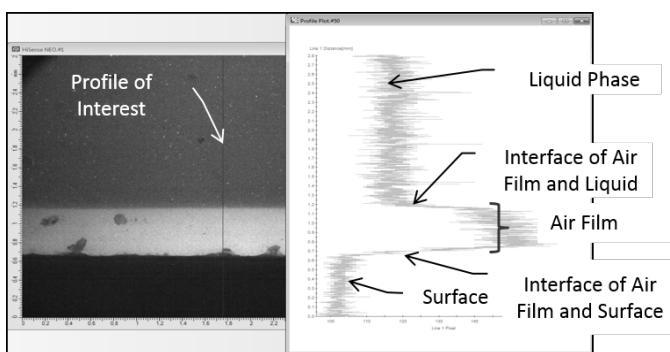


Fig. 1 Image of the air film layer captured by the microscope and analyzed for air layer identification

The brightness difference of the liquid and air film is clearly visible. The border of two phases can be determined with pixel accuracy. It was proven, that the air film layer strongly depends on Re number, respectively of the flow velocity.

Conclusiveness of this visualization was validated with the fluorescent method. The water was colored with fluorescence dye (Rhodamine 6G), that is concentration sensitive and the air film was visualized in the green laser light (532 nm) for the excitation. The emitted light gave us information about local concentration and the relation between water and gas. The air film was seen as a very dark region. This means there was no concentration of the fluorescent dye in this layer. The transition between water and air film was analyzed as difference of brightness in selected region. We processed the image using the plot analysis. The plot was set across the whole image height. The example of the result is seen on figure 1. There is difference between liquid phase and air film can be recognized as step change of brightness. It is

characterized as two interfaces: first between liquid and air, the second between air and ultra-hydrophobic surface. There was used dimensional calibration, so we could precisely measure the air film formed between these two interfaces.

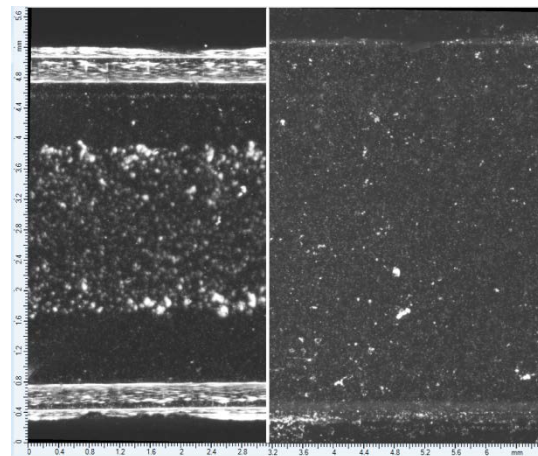


Fig. 2 View into the PCB channel: left side - air film upon the walls with the fluid flow  $Re = 300$ , right side - the same channel with the  $Re = 3000$  - clear walls without air film

The formation of air is dependent on the contact angle. Here in our study we worked with hydrophobic surfaces, with contact angle (CA) above  $90^\circ$ , and with ultra – hydrophobic surfaces with CA above  $120^\circ$ . Increasing the contact angle leads from bubbles conglomeration to uniform air film. So far, the air film was observed as the static effect, which means no liquid flow above the surface. The effect of increasing flow rate is seen in figure 2. There is selected three images of the channel sample B. The initial air film of thickness 370  $\mu\text{m}$  is fluently decreasing to zero.

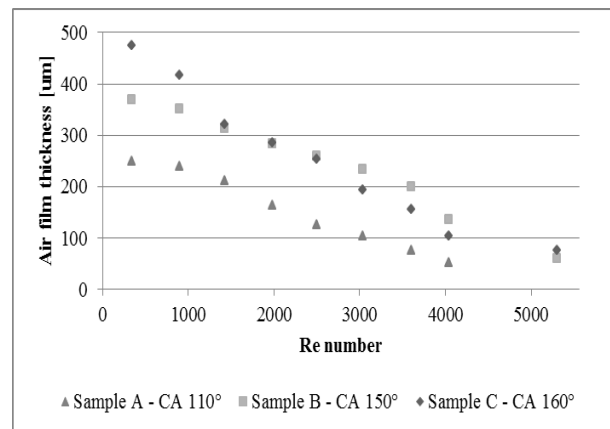
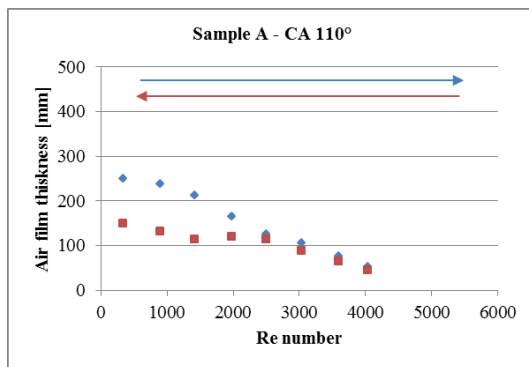


Fig. 3 Comparison of air film thickness is depending on Reynolds number of the liquid flow for selected samples with various CA

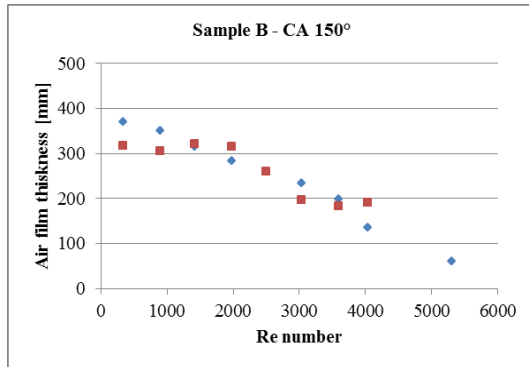
The existence of symmetrical air layer close to hydrophobic surface has an effect on the character of the velocity profile. The air layer reduces the lumen cross section. This takes effect on resulting maximal velocity over flow profile, although maintaining a constant speed of the pump. The maximal differences could be seen in laminar zone. The thickness of air film for  $Re = 340$  reaches for sample A up to 250  $\mu\text{m}$  that

reduces the lumen cross section to 82%, for sample B 360  $\mu\text{m}$ , that means 75%, and for sample C the air film thickness is 470  $\mu\text{m}$ , so the reduces are to 68% of full cross section area. So the Reynolds number used for similarity expression requires to be recalculated.

a)



b)



c)

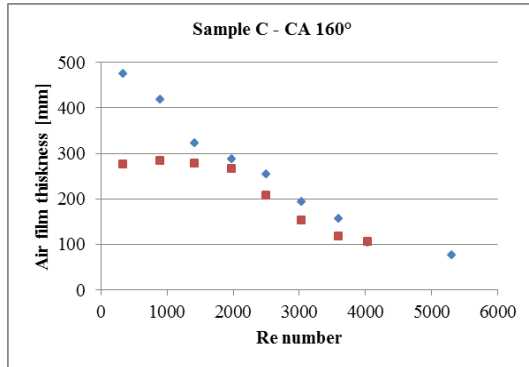


Fig. 4 Graphs of decreasing of air film according to Re number for samples of various initial contact angle a) CA=110°, b) CA = 150°and c) CA=160°

The existence of air film is dependent on the fluid flow velocity. If the velocity exceeds value for laminar or transient Reynold number, it will start decreasing, but will not totally disappear. According to Cassies theory the gas is snoozed into pores of the surface, or change density of boundary stratified layer of liquid.

We processed the measurement with increasing and

decreasing Reynolds number to prove this theory. The resulting air film thickness is seen in Fig. 3. There was not exceeded critical Re number in all three cases. The critical number was set 5000. The flow in this region is characterized as turbulent. There is seen significant diminution between initial air film thickness and at the end of experiment. We can not characterize this diminution correlated to initial contact angle. Anyway, if the channel is relaxed and dry out totally, the air film moves to the initial values.

The second part of our experimental work was dealing with the velocity profile estimation in the cross section of the channel. Air film could be only several micrometers thick, but takes effect in velocity slip close to the surface. This theoretical postulate required experimental prove. We set two areas of interest according to Reynolds number. Firstly it was chosen the flow in laminar zone (Re 153), and the second was set in turbulent (Re 13000). We expected no significant change in velocity profile close to the surface, as we have already know, that the critical Re number for air film is 5000.

The velocity profiles were measured on 3 samples for each material. We worked with ceramic surface modification (marked as Ceramic Surface), with CA 100°. The second set of three samples was covered with Ceramic Surface and ultra-hydrophobic material that is not very mechanically resistant, but reach CA 150° (marked as Ceramic Surface + UH). The reference were left uncoated (marked as Steel Samples) with CA 60°, and also with ultra-hydrophobic surface (Steel + UH).

The resulting velocity profiles are average value calculated from repeated measurement on three samples. The mean standard deviation is less than 5% for single velocity point. This error is partly caused by the method error and partly the flow instabilities over the time of measurement.

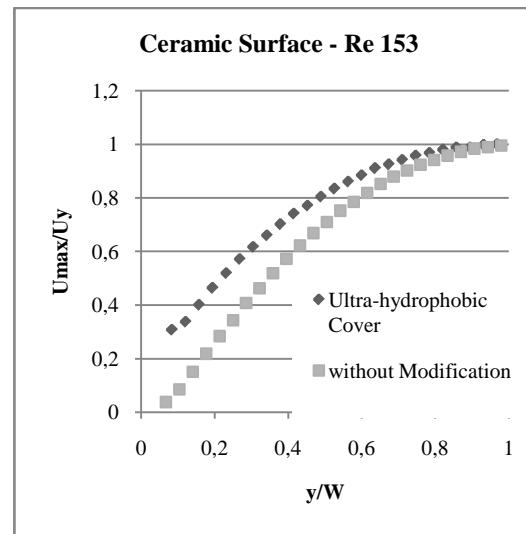


Fig. 5 Comparison of velocity profiles over the channel width and Re 153. Channel surface primary covered with ceramic

Velocity profiles are standardized to the central line velocity ( $U_{\max}$  for laminar zone) and calculated for each  $U$  related to  $y$ , marked as  $U_y$ . The  $y$  axis is the distance from the surface over the cross section width  $W = 8 \text{ mm}$ . The position  $y$  in cross section is also related to width of the channel. The

presence of air film is influencing the velocity profile. The gap is seen in figure 5. The air film is formed close to ultra-hydrophobic cover, so the velocity profile starts in corresponding distance. Effect of air film presence takes shape in the starting point of the velocity profile, means the first valid vector close to the air film, as the boundary slip.

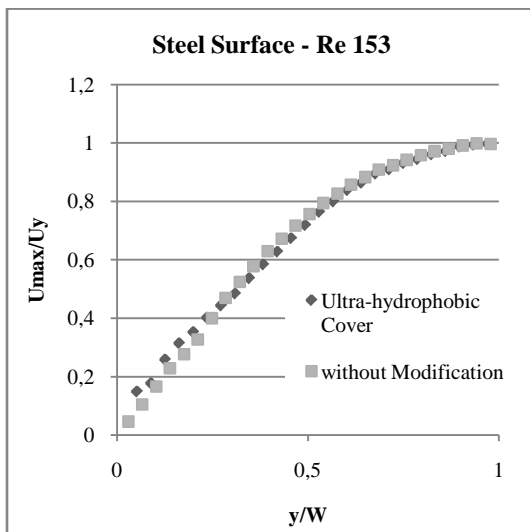


Fig. 6 Comparison of velocity profiles over the channel width and Re 153

Ultra-hydrophobic surface influences besides the starting point of the profile also the shape of the velocity profile. With low Re numbers and air film layer thicker than dozens of micrometers, some interphase interactions are expectable. Friction between solid wall and liquid is extended to solid wall – air layer and air layer – liquid friction processes. For this time, there is no method to determine the velocity profile in the air film, but it must grow differently than the velocity profile of liquid directly on the wall. Accepting that assumption, we did not expect any velocity profiles changes with the flow over Re 5000, because there is now visible air film layer. Velocity profiles of the flow in the channels with different surfaces are presented on the Fig. 7 and Fig. 8.

Figure 7 represents the velocity profile above the material unattended with ultra-hydrophobic layer. Contact angles of the steel without treatment and steel with ceramic surface stay under 90 degrees for pure steel and 120 degrees for steel with ceramic surface. Velocity profiles follow the standard “zero speed condition” on the solid wall. Ceramic surface provides slightly higher velocity close to the surface than the untreated steel. Comparing the velocity profiles measured close to unmodified surface, there is no significant slip. The profiles follow the standard turbulent shape of velocity profile. The first valid vector contains the area of 32 px of the image taken just above the surface line. Results of PIV method are averaged in interrogation area with the dimension depending on the scale factor that taken in account.

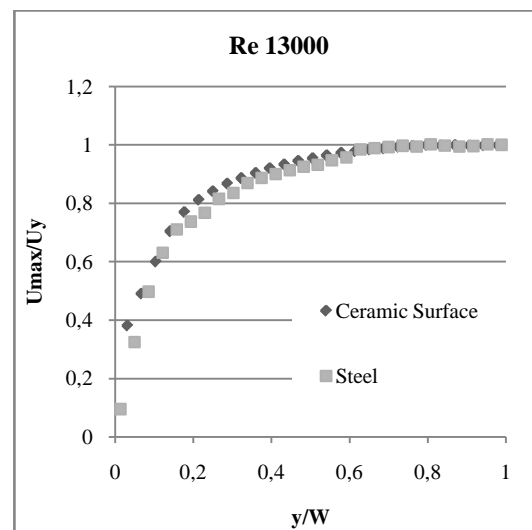


Fig. 7 Comparison of velocity profiles over the channel width and Re 1300 for ceramic surface and steel without hydrophobic cover

Measurement of the flow with high Reynolds number on ultra-hydrophobic coated surfaces provided results with significant shift of the velocity profiles. Profiles on Fig. 8 proved rapidly growing velocities close to the wall. Of course, there are limits of the PIV resolution, but the velocities with distance of 50  $\mu\text{m}$  are much higher than zero. They are reaching 0.5x of the maximum channel velocity. As was already mentioned, the air film is not visible with that Re numbers, but ultra-hydrophobic layer still influences the flow. High Re number with high flow rate and pressure stuff the pores of the walls with the air. The roughness of the wall looks finer, maybe a very thin (not able to see and measure) air layer stays there. All these results prove the slip of the water on the ultra-hydrophobic surface.

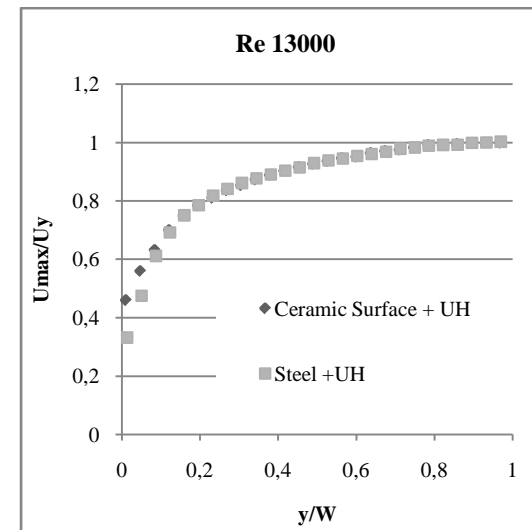


Fig. 8 Comparison of velocity profiles over the channel width and Re 1300 for ceramic surface and steel, both with additional hydrophobic modification

## IV. CONCLUSION

Here we proved the existence of the air film close to the ultra-hydrophobic surfaces. We estimated its thickness depending on Reynolds number that represents the flow rate of the liquid. The method of optical investigation was adjusted for air film thickness determination. Image analysis was used to evaluate the data of air film layer in the water channel. Dynamic interaction of the liquid with ultra-hydrophobic surface is accompanied by formation of a layer of air film.

The proof of the quality of air film belongs to one of dynamic characteristics of ultra-hydrophobic surfaces. So far, the ultra-hydrophobic surfaces were described only by static method, measuring contact angle. However, sometimes the ultra-hydrophobic surfaces are not achieving the expected behavior in the dynamic interaction with liquids, although their CA is higher than 150°. The parameters and the quality of the air film are dependent on the quality and uniformity of hydrophobic surface, which results from the basic characteristics of skin friction. As the dynamics of fluid flow is acting on the air film, the air film is influencing the character of liquid interaction as well as the maximal velocity of the flow. Study described velocity profiles above the ultra-hydrophobic surface; significant shift of these velocity profiles was proved. On low flow rates ( $Re < 1000$ ) the velocity profile of the water does not start immediately by the solid wall, but is measurable from the interface air film-water. Velocities grow faster, what was seen on Fig. 5. On high Re numbers the flow did not follow the standard turbulent profile of channel flow, but contained non-zero velocities close to the wall. First measured velocity was in the distance of 50 $\mu\text{m}$ . These results did not prove the slip effect on ultra-hydrophobic surface yet, there can still be a very thin boundary layer (micrometers) with extreme profile gradient, but there is significant change of velocity profiles compared to non-hydrophobic material. The presence of air film could cause problems with blood clotting, but the boundary slip close to wall can influence the form of erythrocytes distribution in this two phase flow. This will be next step of our research.

## REFERENCES

- [1] T. Hayat, F. M Abbasi, B. Ahmad, A. Alsaedi, "Peristaltic transport of Carreau-Yasuda fluid in a curved channel with slip effects", Plos One 9 (4), 2014.
- [2] P. Crosetto, P. Reymond, S. Deparis, Kontaxakis, N. Stergiopoulos, A. Quarteroni, "Fluid-structure interaction simulation of aortic blood flow", Comp&Fluids 43, 2013, pp. 46-57.
- [3] J. Janela, A. Moura, A. Sequeira, "A 3D non-Newtonian fluid-structure interaction model for blood flow in arteries", J Comp App Math 234, 2010, pp. 2783-2791.
- [4] D. Tang, Z. J. Yang, P. K. Woodard, G. A. Sicard, J. E. Saffliz, C. Yuan, "3D MRI-based multicomponent FSI models for atherosclerotic plaques", Ann Biomed Eng. 32, 2004, pp. 947-960.
- [5] H. Schlichting, K. Gersten, *Boundary Layer Theory*, Springer, Berlin 2000.
- [6] A. J. M. Spencer, *Constitutive theory for strongly anisotropic solids. Continuum Theory of the Mech of FibreReinf Compos*, Springer Verlag: Vienna, Austria, 1984.
- [7] B. Schmandt, H. Herwig, "Loss Coefficients for Periodically Unsteady Flows in Conduit Components: Illustrated for Laminar Flow in a Circular Duct and a 90 Degree Bend", J.Fluids Eng 135(3), 2013, pp. 031204/1-031204/9.
- [8] M. Campolo, M. Simeoni, R. Lapasin, A. Soldati, "Turbulent Drag Reduction by Biopolymers in Large Scale Pipes", J. Fluids Eng 137(4), 2015, pp. 041102/1-041102/10.
- [9] H. Stel, A. T. Franco, S. L. M. Junqueira, R. H. Erthal, R. Mendes, M. A. L. Gonçalves, R. E. M. Morales, "Turbulent Flow in D-Type Corrugated Pipes: Flow Pattern and Friction Factor", J. Fluids Eng 134(12), 2012 pp. 121202/1- 121202/9.
- [10] W. T. Wu, N. Aubry, M. Massoudi, J. Kim, James F. Antaki, "A numerical study of blood flow using mixture theory", International Journal of Engineering Science 76, 2014, pp. 56-72.
- [11] M. Massoudia, J. Kimb, J. F. Antakib, "Modeling and numerical simulation of blood flow using the theory of interacting continua", International Journal of Nonlinear Mechanics 47 (5), 2012, pp. 506-520.
- [12] D. Gidaspow, *Multiphase flow and fluidization: continuum and kinetic theory descriptions*. New York: Academic Press; 1994.
- [13] J. Jung, A. Hassanein, R. W Lyczkowski, "Hemodynamic computation using multiphase flow dynamics in a right coronary artery", Ann Biomed Eng 34, 2006, pp.393-407.
- [14] F. E. R. Corredor, M. Bizhani, E. Kuru, "Experimental investigation of drag reducing fluid flow in annular geometry using particle image velocimetry technique", Journal of Fluids Engineering 137 (8), 2015, pp. 1070-1078.
- [15] H. Ozohul, P. Jay, A. Magnin, "Slipping of a viscoplastic fluid flowing on a circular cylinder", J. of Fluids Engineering 137(7), 2015.
- [16] K. J. Hammad, "The Flow Behavior of a biofluid in a separated and reattached flow region", J. of Fluids Engineering 137(6), 2015.
- [17] P. Skacel, J. Bursa, "Comparison of constitutive models of arterial layers with distributed collagen fibre orientation", Acta of Bioengineering and Biomechanics 16 (3), 2014.
- [18] P. Skacel, J. Bursa, "Poisson's ratio of arterial wall – inconsistency of constitutive models with experimental data", Journal of the Mechanical Behavior of Biomedical Materials. 54, 2016, pp. 316-327.
- [19] S. Polzer, T. C. Gasser, K. Novak, V., Man, M. Tichy, P. Skacel, J. Bursa, "Structure-based constitutive model can accurately predict planar biaxial properties of aortic wall tissue", Acta Biomaterialia 14, 2015, pp. 133-145.
- [20] S. Polzer, T. C. Gasser, J. Swedenborg, J. Bursa, "The Impact of Intraluminal Thrombus Failure on the Mechanical Stress in the Wall of Abdominal Aortic Aneurysms", Eur J Vasc Endovasc Surg, 41, 2011, pp. 467-473.
- [21] S. Polzer, J. Bursa, T. C. Gasser, R. Staffa, R. Vlachovsky, "A numerical implementation to predict residual strains from homogenous stress hypothesis with application to abdominal aortic aneurysms", Ann Biomed Eng. 41, 2013, pp. 1516-1527.
- [22] S. Polzer, T. C. Gasser, C. Forsell, H. Druckmüllerova, M. Tichy, R. Staffa, R. Vlachovsky, J. Bursa, "Automatic Identification and Validation of Planar Collagen Organization in the Aorta Wall with Application to Abdominal Aortic Aneurysm", Microsc Microanal 19, 2013, pp. 1395-1404.
- [23] S. Fialová, M. Hudec, F. Pochylý, et al., "Experimental Verification of the Use of UltraHydrophobic Materials for Water Aeration", Internationa Journal of Advancements in Technology 6 (2), 2015, pp. 1000141-1000147
- [24] S. Fialova, F. Pochylý, "Identification and experimental verification of the adhesive coefficient of Hydrophobic Materials", Wasserwirtschaft 1, 2015, pp.125-129.
- [25] F. Pochylý, H. Krausova, S. Fialova, "Application of the Shannon – Kotelnik theorem on the vortex structures identification", Earth and Environmental Science.IOP Conference Series: Earth and Environmental Science. Montreal: IOP Publishing, 2014, pp. 1-11.
- [26] F. Pochylý, E. Malenovsky, L. Pohanka, "New approach for solving the fluid-structure interaction eigenvalue problem by modal analysis and the calculation of steady-state or unsteady responses", J. of Fluids and Structures 37, 2013, pp. 171-184
- [27] E. E. Meyer, "Recent progress in understanding hydrophobic interactions", PNAS 103, 2006, pp. 15739-15746
- [28] C. Tropea, A. L. Yarin, J. F. Foss, *Handbook of Experimental Fluid Mechanics*, Springer-Verlag Berlin Heidelberg, 2007.
- [29] N. I. Kolev, *Multiphase Flow Dynamics 3*, Springer-Verlag Berlin Heidelberg, 2007.